

Ab-initio structure and dynamics of supercritical CO₂

Wenhui Mi,^{1, a)} Pablo Ramos,^{1, b)} Jack Maranhao,¹ and Michele Pavanello^{1, 2, c)}

¹⁾*Department of Chemistry, Rutgers University, Newark, NJ 07102, USA*

²⁾*Department of Physics, Rutgers University, Newark, NJ 07102, USA*

(Dated: 30 November 2021)

Green technologies rely on green solvents and fluids. Among them, supercritical CO₂ already finds many important applications. The molecular level understanding of the dynamics and structure of this supercritical fluid is a prerequisite to rational design of future green technologies. Unfortunately, the commonly employed Kohn-Sham DFT is too computationally demanding to produce meaningfully converged dynamics within a reasonable time and with a reasonable computational effort. Thanks to subsystem DFT, we analyze finite-size effects by considering simulation cells of varying sizes (up to 256 independent molecules in the cell) and finite-time effects by running 100 ps-long trajectories. We find that the simulations are in reasonable and semiquantitative agreement with the available neutron diffraction experiments and that, as opposed to the gas phase, the CO₂ molecules in the fluid are bent with an average OCO angle of 175.8°. Our simulations also confirm that the dimer T-shape is the most prevalent configuration. Our results further strengthen the experiment-simulation agreement for this fluid when comparing radial distribution functions and diffusion coefficient, confirming subsystem DFT as a viable tool for modeling structure and dynamics of condensed-phase systems.

^{a)}Electronic mail: wenhui.mi@rutgers.edu

^{b)}Electronic mail: p.ramos@rutgers.edu

^{c)}Electronic mail: m.pavanello@rutgers.edu

Supercritical CO₂ is emerging as an important fluid for green technological applications ranging from refrigeration to solvation, and oil extraction^{1,2}. Thus, understanding its properties at the molecular level is very important as it enables the rational development of future technologies. While liquids such as liquid water³⁻⁵ have been extensively studied with a large array of ab-initio electronic structure techniques, the molecular-level structure and dynamics of supercritical CO₂ has not enjoyed a similar interest from the modeling community, probably because of the high computational complexity involved in the simulations (e.g., CO₂ molecules are more extended than H₂O molecules and carry a larger number of electrons) unless very high pressures are considered⁶. However, ab-initio models⁷⁻¹⁰ and experiments based on neutron diffraction¹¹⁻¹³ and X-ray scattering^{14,15} are available and classical molecular dynamics (MD) simulations carried out with force-fields have also been presented^{9,10}. The simulations so far have largely resulted in qualitative agreement with the experiments. Particularly interesting has been the work by Balasubramanian et al.⁹ finding that by improving the employed force field (fitting against coupled cluster energies), a shoulder appears in the C–O radial distribution function (RDF) which is due to prevalent T-shape geometries in the fluid^{8,10}.

Thus, details of the structure of supercritical CO₂ are still largely to be debated and in this work we make significant headway in the analysis of the structure of the fluid as well as its dynamics. Particularly in regards to the latter, by running simulations on a large simulation cell containing 256 independent CO₂ molecules we reduce the inconvenient effects of thermostats on the dynamics. And by running dynamics for 100 ps on a medium-sized simulation cell containing 32 independent CO₂ molecules, we access converged structural parameters.

Long-time dynamics as well as large simulations cells are difficult to approach because ab-initio quantum mechanical models are computationally expensive and a large number of processing units along with a large amount of memory are generally needed to carry out converged simulations. For example, Kohn-Sham DFT (KS-DFT) computational complexity typically scales with the cube of the number of electrons considered^{16,17} while the memory grows quadratically. Doubling the cell size would make the KS-DFT calculation eight-fold more complex. To ameliorate the computational scaling, in this work we employ subsystem DFT¹⁸⁻²⁰ (sDFT, hereafter), a density embedding method that results in a divide and conquer algorithm which effectively scales almost linearly^{21,22}.

The crucial difference between sDFT simulations and KS-DFT is the fact that to achieve a subsystem partition at the level of the energy functional, it is necessary to invoke nonadditive kinetic energy functionals (NAKE)^{23–25}. GGA NAKEs are typically implemented, as they provide a good compromise between accuracy and efficiency of the associated algorithms^{20,26–28}. In sDFT, the electron density is additive²⁵, $\rho(\mathbf{r}) = \sum_I^{N_S} \rho_I(\mathbf{r})$, with N_S being the number of subsystems. With that, we solve for N_S coupled KS equations, one per subsystem

$$\left[-\frac{1}{2}\nabla^2 + v_s^I(\mathbf{r}) + v_{emb}^I(\mathbf{r}) \right] \phi_i^I(\mathbf{r}) = \varepsilon_i^I \phi_i^I(\mathbf{r}), \quad (1)$$

where $v_s^I(\mathbf{r})$ is the KS potential of the isolated subsystem I , while $v_{emb}^I(\mathbf{r})$ is the embedding potential for the same subsystem defined as the functional derivative of all the nonadditive functionals (Coulomb, exchange–correlation and NAKE). By solving the equations in Eq.(1) independently on separate sets of CPUs for each subsystem, sDFT computer codes exploit parallel computer architectures^{21,22} and the locality of the electronic structure²⁹.

Our embedded Quantum ESPRESSO (eQE) software²¹ implements sDFT in an efficient way achieving almost perfect parallel scaling in large part because the only quantity that needs broadcasting is the electron density (an order- N quantity). eQE has been employed before for simulations of large systems providing a quantitative model at a much reduced computational cost compared to KS-DFT of the supersystem both for ground state simulations (which include simulations of liquid water)^{29–31} as well as simulations of excited states dynamics^{32–35}.

In this work, the KS-DFT calculations are carried out with Quantum-ESPRESSO (QE)³⁶ and sDFT with eQE. The electronic structure is computed at the Γ –point, and ions are described with ultrasoft pseudopotentials³⁷ (from Quantum-ESPRESSO library). Energy cutoffs of 40 Ry for the plane wave expansion of the electronic wavefunctions, and 400 Ry for the charge density are employed. We present two simulation setups. The first has 32 CO₂ molecules in a cubic box of lattice vector $a = 15.0 \text{ \AA}$ (CO32, hereafter). In the second set of simulations we increase the system size eight-fold, 256 CO₂ molecules in a cubic box of $a = 30.0 \text{ \AA}$ (CO256, hereafter). To our knowledge, CO256 is the largest system size considered so far for fluid CO₂ by an ab-initio electronic structure method.

Born-Oppenheimer ab-initio molecular dynamics (AIMD) simulations are run with a time step of 30 a.u. driven by the Verlet propagator. The temperature is kept at 314 K

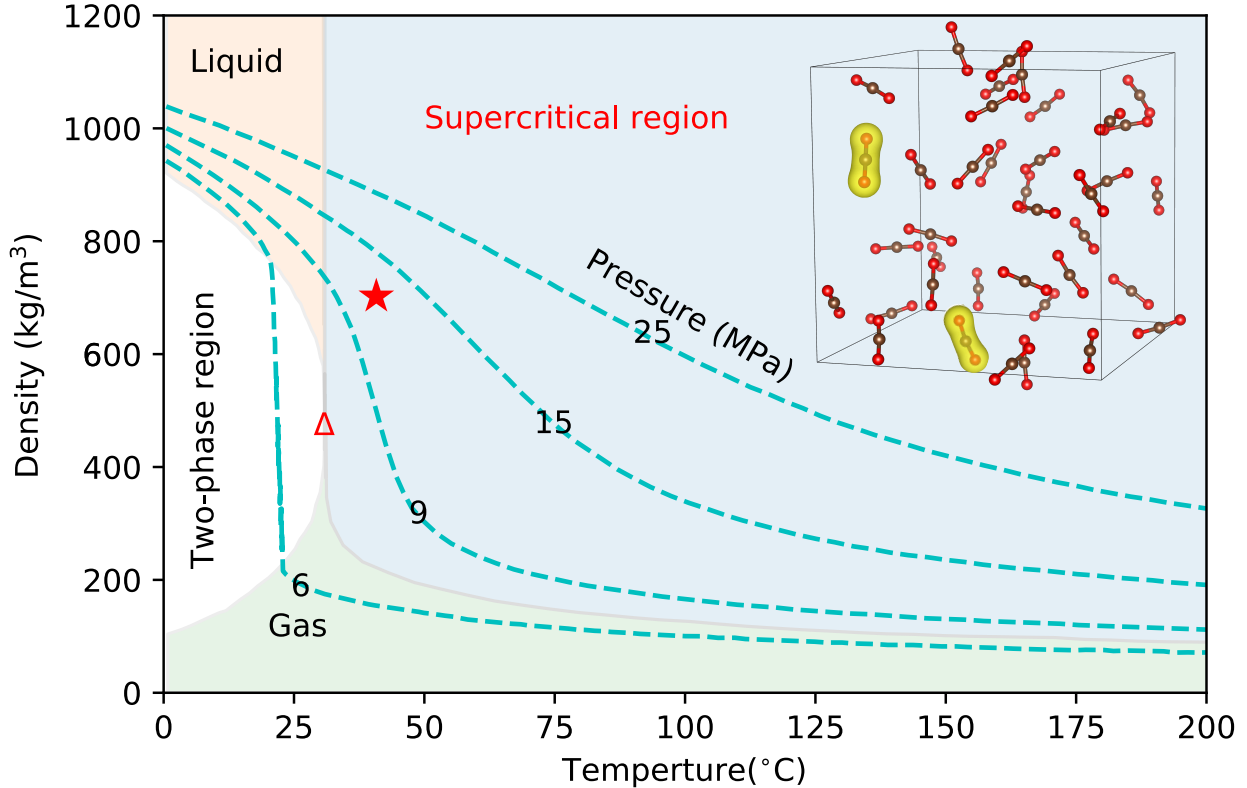


FIG. 1: Phase diagram of CO₂ in the region of the supercritical liquid. The red star indicates the chosen simulation conditions and the triangle indicates the triple point. In inset, the CO₂ simulation cell including a depiction in yellow of two CO₂ molecule subsystem electron densities.

± 30 K using a velocity rescaling thermostat. In addition to the sDFT simulations, we also run KS-DFT simulations on the CO₂ system with the PBE³⁸ exchange–correlation functional. These are indicated by KS-PBE, hereafter. The energy drift during the dynamics was recorded to be as low as 1.2 meV/molecule/ps (see Figure S1 of the supplementary materials³⁹).

Similarly to a previous study for liquid water³¹, we employ subsystem-specific simulation cells only to expand the KS orbitals of the subsystems and to represent the subsystem Hamiltonian. These cells are subsystem-centered and have a lattice vector 40 % the size of the native simulation cell for the CO₃₂ system and 20 % for the CO₂₅₆ system. This is so for every subsystem and in overall this procedure allows the reduction of the total number of plane waves in the calculation by 94 % and 99 % for CO₃₂ and CO₂₅₆, respectively. Specific details of this implementation in eQE can be found elsewhere³¹. In all AIMD simulations, the first 5000 steps are discarded, the remaining steps are used for data analysis and generation

of the results.

While the CO32 sDFT simulations run for 100 ps, the CO32 KS-PBE simulations run for 30 ps. The sDFT simulations of the CO256 system were restarted from a 65 ps CO32 sDFT dynamics and were run for an additional 10 ps.

In Figure 2 we indicate with a red star the place in the phase diagram where our simulations locate. We also show a picture of the simulation cell of the CO32 system with highlighted two subsystem electron densities. Under the simulation conditions, our supercritical CO₂ model system is at the edge between the liquid-gas phase and the supercritical region.

TABLE I: Most probable intra/intermolecular (first solvation shell only) interatomic distances in Å. Diffusion coefficient, D , in units of $10^{-8}m^2/s$.

Bond	Experiment	KS-PBE	sDFT ^d	sDFT ^e
Intramolecular				
C-O	1.17 ¹³	1.17	1.17	1.17
O-O	2.33 ¹³	2.35	2.34	2.34
Intermolecular				
C...C	4.05 ^a / 4.01 ^b	4.47	4.02	4.02
C...O	4.11 ^b	4.29	4.12	4.10
O...O	3.24 ^b	3.52	3.20	3.24
D	3.6-4 ^c	3.1	4.5	4.2

^a Based on Ref. 13, the peak position of RDF at 4.05 Å at $P = 10.2$ MPa in the experiment.

^b Based on Ref. 12, experiment and MD simulation analysis.

^c Using data from Ref. 40, we extrapolate the diffusion coefficient at the temperature and pressure condition of the simulations to be between 3.6 and $4.0 \times 10^{-8}m^2/s$.

^d CO32: 32 independent CO₂ molecules.

^e CO256: 256 independent CO₂ molecules.

In Table I, we show the most probable interatomic distances as they are sampled during the molecular dynamics. The KS-PBE results overestimate the C–C distance by 0.4 Å. These overestimations have been also reported in past ab-initio dynamics based on PBE⁸. While it is difficult to pinpoint the exact origin of this effect, when interactions originating from long-range exchange–correlation are included in the simulation, the most probable C–C distance has been reported to shrink by about 5%⁹. The intramolecular distances are well reproduced by KS-PBE.

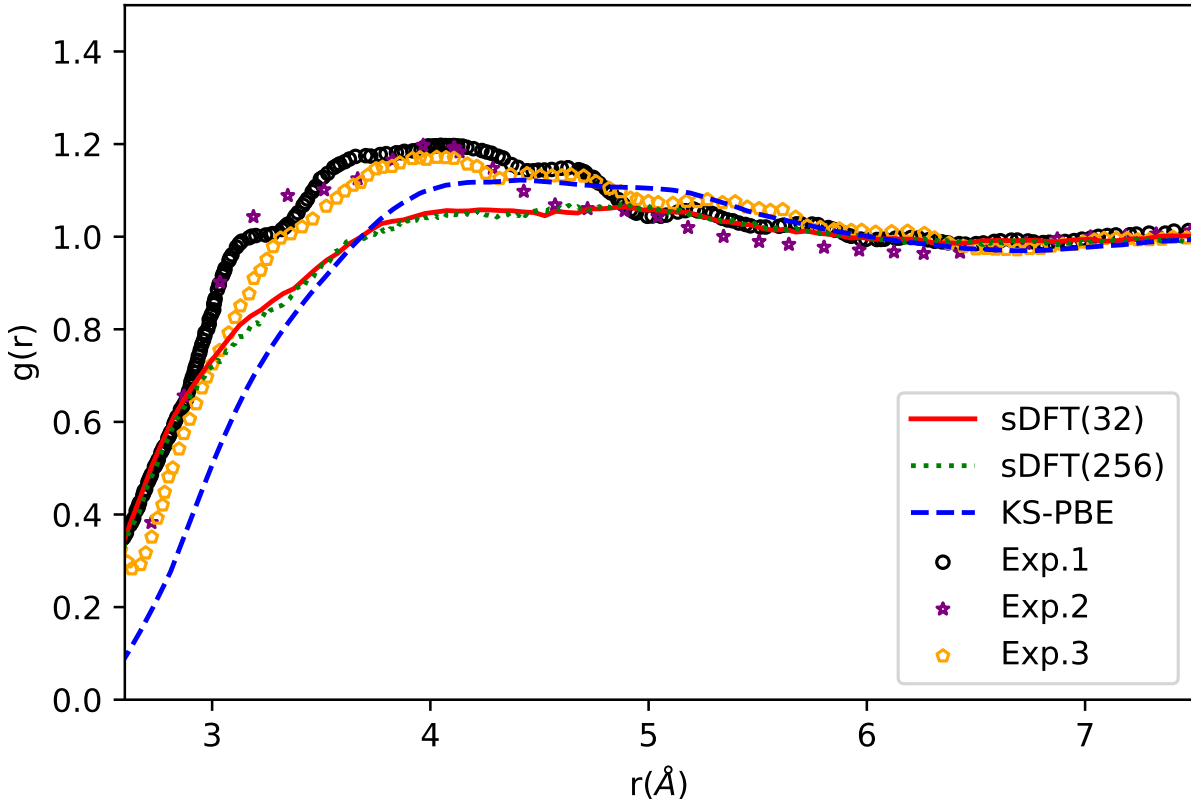


FIG. 2: Full radial distribution function (RDF). Exp. 1-3 are from Refs. 11–13, respectively.

In line with the performance shown for other liquids³¹, the sDFT simulations agree very well with the available experiments for intra and intermolecular distances³¹. The theory-experiment agreement, however, at this stage is only partial as the values of the most probable distances do not offer a full view of the structure of the fluid.

To further assess the quality of the predicted structure of supercritical CO₂, we compute the radial distribution function (RDF) for the entire molecule, presented in Figure 2 (only intermolecular portion is shown). In the figure, we compare three distinct neutron diffraction experiments with our simulations which are in fair agreement with each other. Both KS-PBE and sDFT simulations feature a low density region until about 5 Å. This region is more pronounced for KS-PBE than for sDFT. This possibly indicates that the KS-PBE simulation overstructures the fluid, leaving large empty regions in the structure. An additional indication comes from the diffusion coefficient of the fluid which we compute to be 3.1 for KS-PBE (slightly underestimated) and 4.5/4.1 (slightly overestimated) for sDFT CO32/CO256 (see Table I).

Our results are consistent with the observation that semilocal KS-DFT commonly overstructures molecular liquids due to the detrimental effects caused by the self-interaction error in the inter-molecular interactions^{4,31}.

The C–C, C–O and O–O RDFs are shown in Figure 3 and confirm the analysis given for the total RDF. The sDFT simulations yield a slightly less structured fluid compared to KS-PBE. The onset of the RDFs in the intermolecular region is situated at shorter distances for sDFT compared to KS-PBE. This is also in line with the previously presented water simulations³¹. The main justification for this resides in a documented fallacy of NAKes whereby the equilibrium intermolecular distance between weakly bonded fragments is underestimated^{26,27,41}. However, this feature does not significantly deteriorate the experiment–theory agreement.

A study by Balasubramanian et al.⁹ found that accurate force fields produce a shoulder in the C–O RDF. From Figure 2, we notice that the sDFT simulations and in a somewhat reduced fashion also the KS-PBE simulations produce a shoulder in the $g_{C-O}(r)$. The shoulder indicates that the closest nonbonded oxygen to the carbon is in a distinct configuration compared to the second closest oxygen. This has been attributed to a distorted T-shape geometry^{8,9}. A closer agreement of sDFT with experiments was also noticed in our previous study of water³¹ and we attribute it to the natural error cancellation between the nonpositive nonadditive exchange functional and the nonnegative NAKE. Error cancellation is an important feature of quantum chemistry methods⁴², and in DFT most notably takes place between the exchange and the correlation parts of commonly available exchange–correlation functionals⁴³.

Our simulations support the existence of the T-shape geometry as depicted in Figure 4. In the figure, we show the Θ_T angle between the ABC plane given by the oxygens of one CO₂ and the carbon of another CO₂ molecule with the bond vector form from carbon and oxygen atoms of the latter CO₂ molecule (see caption to Figure 4). Similarly, we study the bond length distribution function of the r_{CO_2--O} intermolecular distance (see Figure 4) within the first solvation shell.

The angular distribution function (ADF) of the angle θ_T is displayed in Figure 5, it is clear that the most probable geometry shown in this ADF is the T-shape form. However the distribution is far from being sharp, corroborating previous studies⁹. To further shed light on this aspect, we computed the bond length distribution function of the distance r_{CO_2--O}

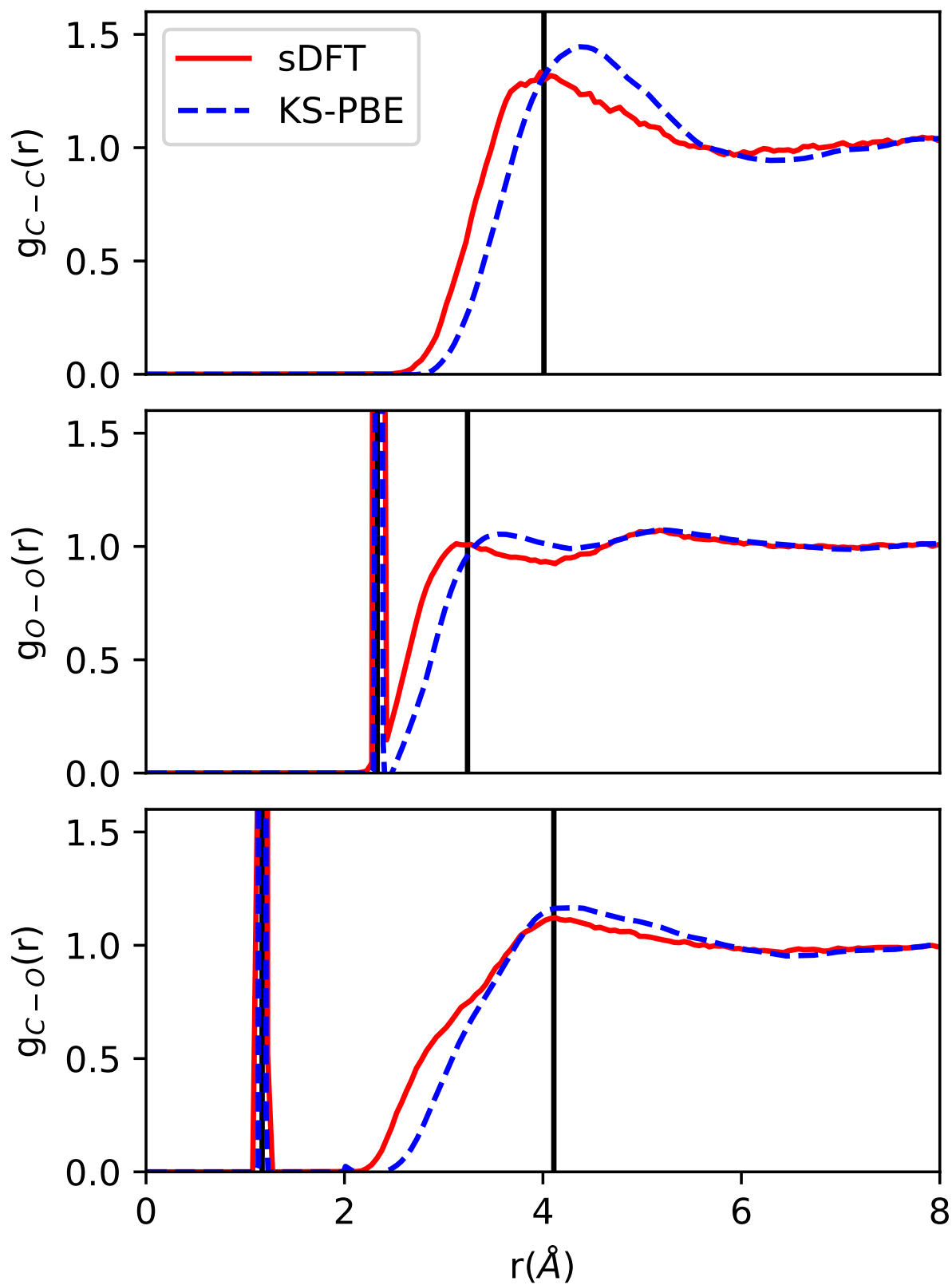


FIG. 3: C-C, C-O, and O-O radial distribution functions (RDFs). The experimental most probable interatomic distances are indicated by the black vertical line. The strong, sharp peaks occur at the intramolecular distances. CO32 and CO256 gave equivalent RDFs. Here we show RDFs computed for CO32.

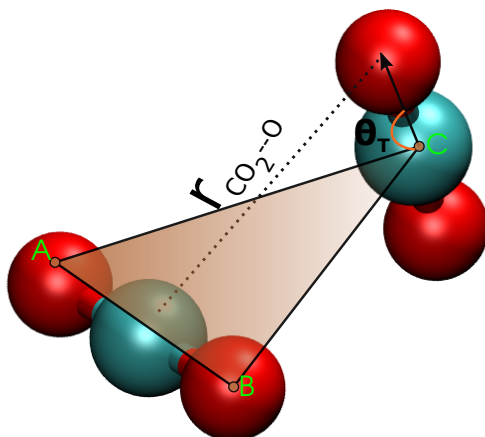


FIG. 4: Intermolecular parameters computed within the first solvation shell used to elucidate the most prevalent structural configurations of supercritical CO_2 . The angle θ_T is between plane ABC (given the two oxygen atoms, AB, of one CO_2 and a carbon atom, C, of a nearby CO_2) and the C–O bond vector of the latter CO_2 molecule. The distance $r_{\text{CO}_2--\text{O}}$ is given by the carbon atom of the first CO_2 molecule and one of the oxygen atom from of the second CO_2 molecule.

for three different groups of CO_2 pairs, classified by the angle θ_T : $30^\circ \geq \theta_T \geq 0^\circ$ for group I, $60^\circ \geq \theta_T \geq 30^\circ$ for group II and $90^\circ \geq \theta_T \geq 60^\circ$ for group III, mirror distributions are obtained for angles higher than 90° . We report them in Figure 5. Inspecting the figure, confirms the trend given by the ADF of angle θ_T . I.e., the BDF has two maxima when the angle θ_T is in group I where the difference between the two peaks corresponds to the average of the intramolecular distance between the two oxygen atoms of a CO_2 molecule.

Thus, this clarifies the origin of the shoulder mentioned before in conjunction with the C–O RDF: it is given by the occurrence of T-shaped geometries in which the angle θ_T is close to 0° and a CO_2 molecule is parallel to the plane ABC (see Figure 4). The BDF computed with KS–PBE shows a higher intensity than the sDFT BDF, suggesting that KS–PBE produces a more compact structure than sDFT, in line with Table I and Figure 2.

As mentioned before, an interesting property of supercritical CO_2 is that the molecule bends quite substantially from its linear shape. $\theta_{\text{O–C–O}}$ angular distribution function is shown also in Figure 5. KS–PBE peaks at 177.3° and averages at 176.6° , while sDFT peaks at 176.8° and averages at 175.8° . These are somewhat overestimated compared to the values by Truhlar and coworkers¹⁰ who find average values of 174.5° and a maximum value of 175.7° for KS–BLYP as well as path integral dynamics. However, overall our simulations also

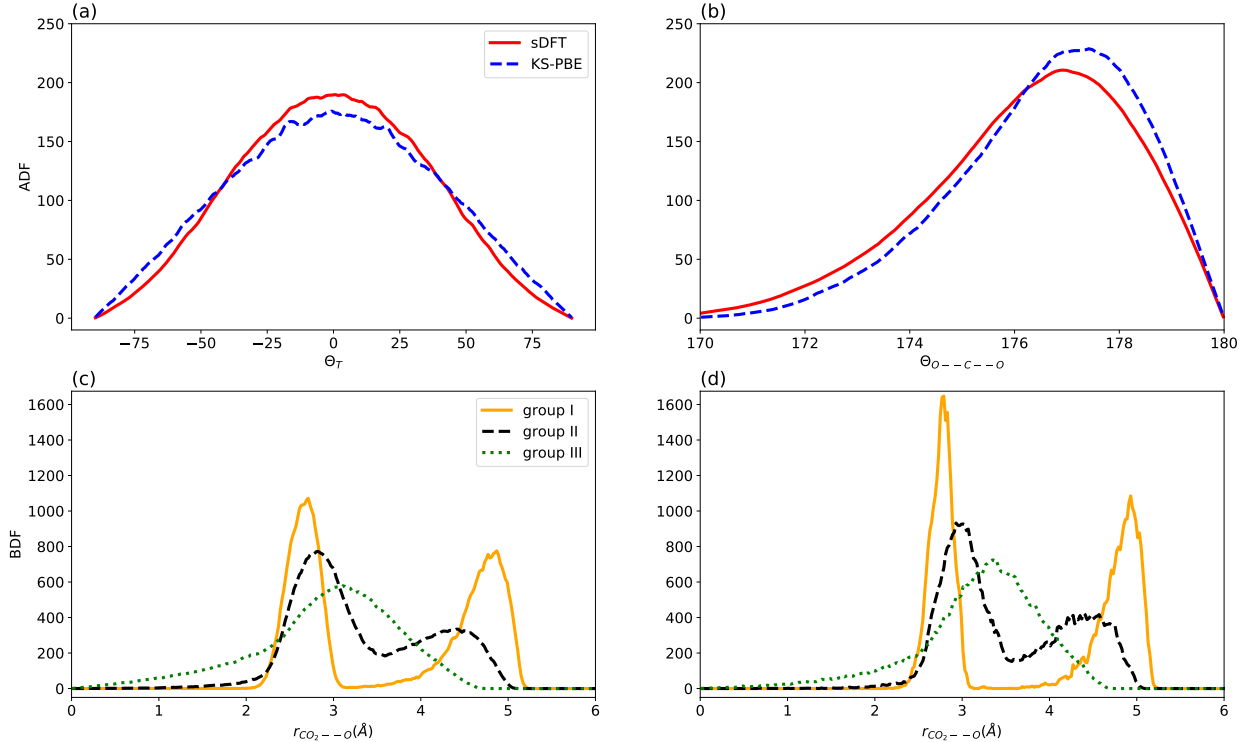


FIG. 5: Computed angular (ADF) and bond length (BDF) distribution functions for supercritical CO₂. (a) ADF for angle θ_T , (b) ADF for the intramolecular θ_{O-C-O} angle, (c) and (d) BDF for the r_{CO_2--O} distance computed with sDFT and KS-DFT respectively. (c) and (d) BDF for the r_{CO_2--O} distance computed with sDFT and KS-DFT respectively.

corroborate the common knowledge that CO₂ molecules are bent when in the supercritical phase.

In conclusion, we carried out ab-initio molecular dynamics simulations of supercritical CO₂. We show that in comparison to KS-DFT with the PBE exchange–correlation functional, subsystem DFT yields a slightly less structured, more diffusive supercritical CO₂ in closer agreement with the available neutron diffraction experiments. Our results support T–shape structure of near-neighbor CO₂ molecules, and the commonly accepted picture that CO₂ molecules spend more time in a bent configuration than in a linear configuration. Our conclusions are supported by 100 ps long Born-Oppenheimer dynamics for the small system, CO32, composed by 32 CO₂ molecules, providing a peace of mind in terms of the convergence of the structural results. The length scales are also probed by considering the CO256 system composed by 256 independent CO₂ molecules, corroborating the results accumulated with the smaller CO32 system.

Our simulations show that subsystem DFT is a viable method for probing time and length

scales that are unattainable by Kohn–Sham DFT of the supersystem. The key resides in the fact that molecular liquids, such as supercritical CO₂, display a localized electronic structure which is well described by subsystem DFT. The eQE codebase leverages these properties and leads to substantial memory and work savings by massively reducing the effective Hilbert space needed to describe the electronic structure by 94 and 99% for the CO32 and CO256 systems (all computed distribution functions for the CO256 system are shown in the supplementary information³⁹), respectively. Locality of the electronic structure is a property shared by several other system types and not just molecular liquids. Thus, we expect the results presented here to be largely transferable to other types of systems (such as layered 2D systems), a topic of current investigation.

ACKNOWLEDGMENTS

This material is based upon work supported by the National Science Foundation under Grant No. CHE-1553993.

REFERENCES

- ¹M. Pieve, G. Boccardi, L. Saraceno, R. Trinchieri, and G. Zummo, “CO₂ transcritical refrigeration cycles: potential for exploiting waste heat recovery with variable operating conditions,” *Journal of Physics: Conference Series* **796**, 012021 (2017).
- ²H. Sovová, “Rate of the vegetable oil extraction with supercritical CO₂: I. Modelling of extraction curves,” *Chemical Engineering Science* **49**, 409–414 (1994).
- ³R. A. DiStasio, B. Santra, Z. Li, X. Wu, and R. Car, “The individual and collective effects of exact exchange and dispersion interactions on the ab initio structure of liquid water,” *J. Chem. Phys.* **141**, 084502 (2014).
- ⁴K. Forster-Tonigold and A. Groß, “Dispersion corrected RPBE studies of liquid water,” *J. Chem. Phys.* **141**, 064501 (2014).
- ⁵M. J. Gillan, D. Alfe, P. J. Bygrave, C. R. Taylor, and F. R. Manby, “Energy benchmarks for water clusters and ice structures from an embedded many-body expansion,” *J. Chem. Phys.* **139**, 114101 (2013).

- ⁶C. Lu, M. Miao, and Y. Ma, “Structural evolution of carbon dioxide under high pressure,” *J. Am. Chem. Soc.* **135**, 14167–14171 (2013).
- ⁷F. Tassone, G. L. Chiarotti, R. Rousseau, S. Scandolo, and E. Tosatti, “Dimerization of CO₂ at high pressure and temperature,” *ChemPhysChem* **6**, 1752–1756 (2005).
- ⁸M. Saharay and S. Balasubramanian, “Evolution of intermolecular structure and dynamics in supercritical carbon dioxide with pressure: an ab initio molecular dynamics study,” *J. Phys. Chem. B* **111**, 387–392 (2007).
- ⁹S. Balasubramanian, A. Kohlmeyer, and M. L. Klein, “Ab initio molecular dynamics study of supercritical carbon dioxide including dispersion corrections,” *J. Chem. Phys.* **131**, 144506 (2009).
- ¹⁰K. E. Anderson, S. L. Mielke, J. I. Siepmann, and D. G. Truhlar, “Bond angle distributions of carbon dioxide in the gas, supercritical, and solid phases[†],” *J. Phys. Chem. A* **113**, 2053–2059 (2009).
- ¹¹R. Ishii, S. Okazaki, I. Okada, M. Furusaka, N. Watanabe, M. Misawa, and T. Fukunaga, “A neutron scattering study of the structure of supercritical carbon dioxide,” *Chem. Phys. Lett.* **240**, 84–88 (1995).
- ¹²P. Cipriani, M. Nardone, and F. Ricci, “Neutron diffraction measurements on CO₂ in both undercritical and supercritical states,” *Physica B: Condensed Matter* **241-243**, 940–946 (1997).
- ¹³R. Ishii, S. Okazaki, O. Odawara, I. Okada, M. Misawa, and T. Fukunaga, “Structural study of supercritical carbon dioxide by neutron diffraction,” *Fluid Phase Equilibria* **104**, 291–304 (1995).
- ¹⁴K. Nishikawa and M. Takematsu, “X-ray scattering study of carbon dioxide at supercritical states,” *Chem. Phys. Lett.* **226**, 359–363 (1994).
- ¹⁵T. Morita, K. Nishikawa, M. Takematsu, H. Iida, and S. Furutaka, “Structure study of supercritical CO₂ near higher-order phase transition line by x-ray diffraction,” *J. Phys. Chem. B* **101**, 7158–7162 (1997).
- ¹⁶J. E. Moussa and A. D. Baczewski, “Assessment of localized and randomized algorithms for electronic structure,” *Electronic Structure* **1**, 033001 (2019).
- ¹⁷D. R. Bowler and T. Miyazaki, “ $O(N)$ Methods in Electronic Structure Calculations,” *Rep. Prog. Phys.* **75**, 036503 (2012).
- ¹⁸T. A. Wesolowski, S. Shedge, and X. Zhou, “Frozen-Density Embedding Strategy for

- Multilevel Simulations of Electronic Structure,” *Chem. Rev.* **115**, 5891–5928 (2015).
- ¹⁹A. Krishtal, D. Sinha, A. Genova, and M. Pavanello, “Subsystem Density-Functional Theory as an Effective Tool for Modeling Ground and Excited States, their Dynamics, and Many-Body Interactions,” *J. Phys.: Condens. Matter* **27**, 183202 (2015).
- ²⁰C. R. Jacob and J. Neugebauer, “Subsystem density-functional theory,” *WIREs: Comput. Mol. Sci.* **4**, 325–362 (2014).
- ²¹A. Genova, D. Ceresoli, A. Krishtal, O. Andreussi, R. DiStasio Jr., and M. Pavanello, “eQE — A Density Functional Embedding Theory Code For The Condensed Phase,” *Int. J. Quantum Chem.* **117**, e25401 (2017).
- ²²C. R. Jacob and L. Visscher, “Density–functional theory approach for the quantum chemical treatment of proteins,” *J. Chem. Phys.* **128**, 155102 (2008).
- ²³G. Senatore and K. R. Subbaswamy, “Density Dependence of the Dielectric Constant of Rare-Gas Crystals,” *Phys. Rev. B* **34**, 5754–5757 (1986).
- ²⁴P. Cortona, “Direct determination of self-consistent total energies and charge densities of solids: A study of the cohesive properties of the alkali halides,” *Phys. Rev. B* **46**, 2008–2014 (1992).
- ²⁵T. A. Wesolowski and A. Warshel, “Frozen Density Functional Approach for *ab Initio* Calculations of Solvated Molecules,” *J. Chem. Phys.* **97**, 8050 (1993).
- ²⁶D. Schlüns, K. Klahr, C. Mück-Lichtenfeld, L. Visscher, and J. Neugebauer, “Subsystem-DFT potential-energy curves for weakly interacting systems,” *Phys. Chem. Chem. Phys.* **17**, 14323–14341 (2015).
- ²⁷A. Götz, S. Beyhan, and L. Visscher, “Performance of Kinetic Energy Functionals for Interaction Energies in a Subsystem Formulation of Density Functional Theory,” *J. Chem. Theory Comput.* **5**, 3161–3174 (2009).
- ²⁸S. Laricchia, E. Fabiano, L. A. Constantin, and F. Della Sala, “Generalized Gradient Approximations of the Noninteracting Kinetic Energy from the Semiclassical Atom Theory: Rationalization of the Accuracy of the Frozen Density Embedding Theory for Nonbonded Interactions,” *J. Chem. Theory Comput.* **7**, 2439–2451 (2011).
- ²⁹A. Genova and M. Pavanello, “Exploiting the Locality of Subsystem Density Functional Theory: Efficient Sampling of the Brillouin Zone,” *J. Phys.: Condens. Matter* **27**, 495501 (2015).
- ³⁰A. Genova, D. Ceresoli, and M. Pavanello, “Periodic Subsystem Density-Functional The-

- ory,” *J. Chem. Phys.* **141**, 174101 (2014).
- ³¹A. Genova, D. Ceresoli, and M. Pavanello, “Avoiding Fractional Electrons in Subsystem DFT Based Ab-Initio Molecular Dynamics Yields Accurate Models For Liquid Water and Solvated OH Radical,” *J. Chem. Phys.* **144**, 234105 (2016).
- ³²S. K. P., A. Genova, and M. Pavanello, “Cooperation and environment characterize the low-lying optical spectrum of liquid water,” *J. Phys. Chem. Lett.* **8**, 5077–5083 (2017).
- ³³A. Krishtal, D. Ceresoli, and M. Pavanello, “Subsystem Real-Time Time Dependent Density Functional Theory,” *J. Chem. Phys.* **142**, 154116 (2015).
- ³⁴A. Krishtal and M. Pavanello, “Revealing Electronic Open Quantum Systems with Subsystem TDDFT,” *J. Chem. Phys.* **144**, 124118 (2016).
- ³⁵A. Umerbekova, S.-F. Zhang, S. K. P., and M. Pavanello, “Dissecting energy level renormalization and polarizability enhancement of molecules at surfaces with subsystem TDDFT,” *Eur. Phys. J. B* **91** (2018), 10.1140/epjb/e2018-90145-2.
- ³⁶P. Giannozzi, O. Andreussi, T. Brumme, O. Bunau, M. B. Nardelli, M. Calandra, R. Car, C. Cavazzoni, D. Ceresoli, M. Cococcioni, N. Colonna, I. Carnimeo, A. D. Corso, S. de Gironcoli, P. Delugas, R. A. D. Jr, A. Ferretti, A. Floris, G. Fratesi, G. Fugallo, R. Gebauer, U. Gerstmann, F. Giustino, T. Gorni, J. Jia, M. Kawamura, H.-Y. Ko, A. Kokalj, E. Kkbenli, M. Lazzeri, M. Marsili, N. Marzari, F. Mauri, N. L. Nguyen, H.-V. Nguyen, A. O. de-la Roza, L. Paulatto, S. Ponc, D. Rocca, R. Sabatini, B. Santra, M. Schlipf, A. P. Seitsonen, A. Smogunov, I. Timrov, T. Thonhauser, P. Umari, N. Vast, X. Wu, and S. Baroni, “Advanced capabilities for materials modelling with q quantum espresso,” *Journal of Physics: Condensed Matter* **29**, 465901 (2017).
- ³⁷A. M. Rappe, K. M. Rabe, E. Kaxiras, and J. D. Joannopoulos, “Optimized pseudopotentials,” *Phys. Rev. B* **41**, 1227–1230 (1990).
- ³⁸J. P. Perdew, K. Burke, and M. Ernzerhof, “Generalized Gradient Approximation Made Simple,” *Phys. Rev. Lett.* **77**, 3865–3868 (1996).
- ³⁹“See Supplementary Material Document at [URL will be inserted by publisher] for additional tables and figures.”
- ⁴⁰P. Etesse, J. A. Zega, and R. Kobayashi, “High pressure nuclear magnetic resonance measurement of spin–lattice relaxation and self-diffusion in carbon dioxide,” *J. Chem. Phys.* **97**, 2022–2029 (1992).
- ⁴¹D. Sinha and M. Pavanello, “Exact Kinetic Energy Enables Accurate Evaluation of Weak

- Interactions by the FDE-vdW Method,” *J. Chem. Phys.* **143**, 084120 (2015).
- ⁴²A. Wasserman, J. Nafziger, K. Jiang, M.-C. Kim, E. Sim, and K. Burke, “The importance of being inconsistent,” *Annual Review of Physical Chemistry* **68**, 555–581 (2017).
- ⁴³M. G. Medvedev, I. S. Bushmarinov, J. Sun, J. P. Perdew, and K. A. Lyssenko, “Density functional theory is straying from the path toward the exact functional,” *Science* **355**, 49–52 (2017).